2024 European Control Conference (ECC)
June 25-28, 2024. Stockholm, Sweden

Experimental Identification of a Lumped-Parameter Thermal Model of a Li-ion Pouch Cell Assembly

Andrea Trivella, Matteo Corno, Stefano Radrizzani, Edoardo Catenaro, Sergio M. Saveresi

Abstract— **Thermal models of lithium-ion cells play a critical role in monitoring temperature distribution within battery packs, sizing cooling systems, and predicting potential thermal runaway scenarios. Pouch-type lithium-ion cells offer high energy and power density solutions, however, they are less thermally and mechanically stable than their cylindrical counterparts. Pouch cells require appropriate containment structures to prevent excessive cell breathing that could alter electrical performance. Experiments done without such holding devices could conceal nominal cell behavior and lack repeatability. The holding structure, on the other hand, influences the heat dissipation of the cell and masks its temperature dynamics, making the characterization of its thermal properties challenging. This paper proposes a lumped-parameter thermal model and an experimental identification protocol aimed at extracting the parameters of interest, such as the cell thermal capacity, using temperature measurements collected both on the cell and fixture device components. The model is trained and validated under current profiles that are highly effective in exciting the system thermal dynamics.**

I. Introduction

The lithium-ion battery industry is experiencing unprecedented growth. Vehicle electrification is pushing manufacturers into continuous technological innovation: new chemistries for high energy density cells [1] [2], lightweight and structural Battery Packs (BPs) [3], and advanced Battery Management Systems (BMSs) for real-time monitoring and optimization of battery operation. Among the various tasks of a BMS, thermal management is one of the most critical [4]: temperature greatly affects the performance and safety of Li-ion cells, and thus of the entire pack. At the cell level, temperature must be kept within a certain threshold to avoid thermal runaways that can eventually produce explosions or fires [5]. The cell temperature can affect its functionality: the internal resistance is highly sensitive to temperature variations [6] and impacts the State of Power (SoP), *i.e.*, the power the cell can deliver at any instant, and the State of Charge (SoC), *i.e.*, the energy available in the cell. In the long run, the working temperature strongly influences the aging of cells [7], and therefore accurate State of Health (SoH) estimators must account for the thermal dynamics. At the pack level, thermal gradients must be monitored to predict and mitigate possible system thermal failures. Hot spots can cause non-uniform distribution of the SoP, SoC, and SoH between cells, thus, BP temperature must be properly regulated through well-sized cooling systems and effective real-time thermal management strategies.

All the authors are with the Dipartimento di Elettronica, Informazione e Bioingegneria, Politecnico di Milano, Via Ponzio 34/5, 20133 Milan, Italy
stefano.radrizzani@polimi.it

In this context, thermal models are indispensable. In the BP design phase, one can simulate the thermal dynamics of cells under different current profiles, analyze temperature distribution in battery packs, or simulate the heat generation for cooling system sizing. In real-time operation, these models can be used to estimate the core temperature of cylindrical cells [8], software-sense the temperature of certain cells to reduce the number of sensors in the pack, detect abnormal temperature elevations to predict thermal failures, and so on. Two kinds of models are typically used for Li-ion cells: white-box electrochemical models and empirical reduced-order models. The former couple a classical physics-based model such as a Single Particle Model (SPM), or a Pseudo-Two-Dimensional (P2D) model with temperature dynamics driven by electrochemical reactions [9]. These models are computationally demanding and their non-invasive identification is challenging [10] due to the high number of parameters. Hence, they are mainly used in simulation frameworks for cell design rather than real-time BMS algorithms [11]. In reduced-order models, cell-generated heat is expressed as a function of current, as the joule effect on internal resistance or, in more accurate formulations, as the product between current and overpotential [12]. The temperature distribution over time is then obtained through heat diffusion equations forced by generated heat, convective and conductive terms. The computational complexity of these models depends on the dimensionality and the detail of discretization, but their identification is simpler since they can be represented with a limited number of parameters. The dimensionality is always related to the shape of the cell under analysis. In cylindrical type cells, a 1-D model is preferred: heat diffusion in the radial direction enables the estimation of the core temperature while the temperature distribution along the axial direction is considered uniform [13]. Things are more complex with prismatic cells, where all the three dimensions must be considered, and 3-D models are employed to estimate the core temperature of the prism [14].

Unlike cylindrical ones, pouch cells are commonly tested with ad-hoc fixtures to ensure specified compression pressure [15]: in fact, optimal external pressure on the pouch can both improve its power performance [16] and slow down its capacity fade [17]. Even during the battery pack design, the mechanical compression must be calibrated to ensure safe and optimal performance [18]. As a side effect, the containment structure greatly affects the thermal dynamics of the cell, acting as a heat sink and masking

its actual behavior. Thermal models of different complexity and accuracy have been developed for pouch-type cells. A lumped-parameters 1-D model is coupled with a second-order ECM model and identified by Vertiz et al. [19]. A two-dimensional multi-domain model is developed by Samba et al. [20]: the temperature distribution of tabs, case and cell surface is simulated successfully. Many authors use accurate three-dimensional formulations of heat generation, supported by electrochemical equations, to characterize the thermal dynamics of the pouch cell under analysis [21]–[23]. However, to facilitate the sensing of the device and isolate its thermal properties, the pouch cell was always tested without any compression assembly.

This work proposes a lumped-parameter model and an identification protocol to extract the main parameters of a pouch cell when installed inside a compression assembly. The model assumes that each object of the assembly has a uniform temperature distribution, and captures the heat transfer between them. This modeling approach allows to (*i*) characterize the thermal impact of each element of the fixture and (*ii*) isolate some parameters of interest, such as the thermal capacity of the cell. The innovative contributions in the articles are summarized in:

- the development of an RC-network-based lumped-thermal model of a pouch cell, with overpotential-driven heat generation, and fixture elements;
- the experimental identification and validation of the model for a cell-aluminum-plexiglass testing setup.

The remainder of this document is organized as follows. In Section II, the experimental setup is described and in Section III the model for the setup is proposed. In Section IV the experimental identification procedure and results are presented. Finally, Section V contains the results of the model validation on a different current profile.

II. Experimental Setup

The fixture device has been developed in the laboratories of Politecnico di Milano, Milan, Italy. The pouch cell under test is 140×80×2.5 mm in size (excluding tabs). The cell is packed between two aluminum plates. The plates have a dimension of 240×180×15 mm, hence, covering the entire area of the pouch. They have a dual functionality: (*i*) they uniformly distribute the compression force over the cell surface and (*ii*) they facilitate the dissipation of the heat generated by the cell thanks to their high thermal conductivity. Indeed, the use of low-conductive materials as cell-contact layers could result in significant heat buildup and possible thermal runaway, especially during aggressive current requests. The second layer is composed of 300×300×10 mm plexiglass panels. These panels were installed for several reasons. First, they serve to support the weights of the power cables, which for this application (high discharge currents) are considerably heavy and could, otherwise, damage the cell. Additionally, they provide a layer of electrical insulation between the power elements and the aluminum layer.

Eventually, since they can be easily machined, they facilitate the integration of the elements used for compression (screws and bolts). The latter are used to tighten the setup and ensure the 500 N compression force specified by the cell manufacturer. Fig. 1 shows the fixture described above.

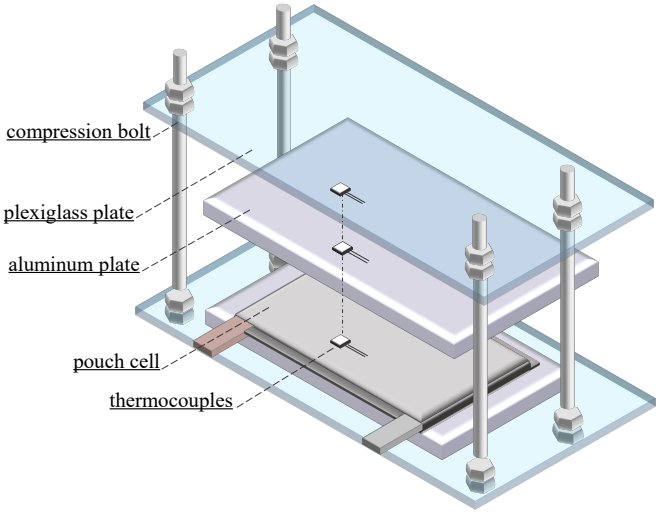

Fig. 1. Illustrative schematics of the cell fixture (dimensional proportions are adjusted for representative purposes).

Three K-type thermocouples are inserted into the setup. The first measures the temperature of the cell and is placed at the center of its top surface. The other two are vertically aligned to the first and measure the temperature of the aluminum block and the plexiglass panel, respectively.

The cell is tested under controlled ambient conditions inside a FDM Environmental Maker that can operate between −20°C and 60°C. The battery testing equipment (BTE) is an ARBIN LBT System with two I-V channels, capable of 5V-500A each. The BTE can apply custom current profiles to the cell and measure current, voltage and temperature at a maximum rate of 1kHz. A computer station is connected via TCP/IP to the BTE and is used to schedule experiments and monitor their progress in real-time via ARBIN software MITS PRO 8. The main elements that compose the test bench are shown in Fig.2.

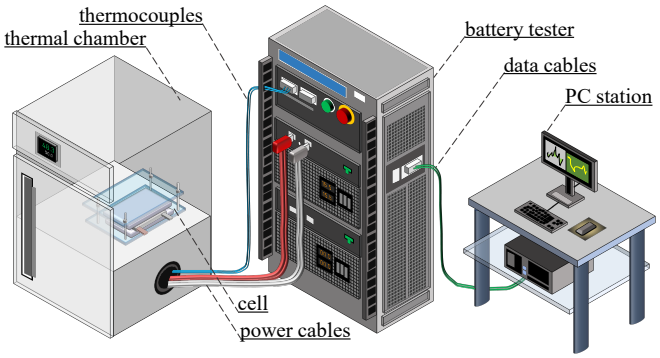

Fig. 2. Illustration of the testing equipment at Politecnico laboratory.

Given the prototypical nature of the cell under test, for confidentiality reasons, the cell specifications and the manufacturer cannot be disclosed, and the graph axes will be normalized. However, considering the generality of the proposed method, the lack of these details does not hinder the reusability for different cells and fixtures.

III. Lumped Thermal Model

The model assumes that each element of the containment structure has a uniform temperature distribution, thus, can be described by a single temperature value. Given a generic object x, its temperature dynamic $T_{\mathrm{x}}(t)$ is defined by the heat balance equation:

$$C_{\mathrm{x}}\frac{\mathrm{d}T_{\mathrm{x}}(t)}{\mathrm{d}t} = q_{\mathrm{x}}(t) + \sum_{\mathrm{y}\in\mathrm{Y}}\frac{T_{\mathrm{y}}(t)-T_{\mathrm{x}}(t)}{R_{\mathrm{xy}}}, \tag{1}$$

where C_{x} [J/K] is the object's thermal capacity, $q_{\mathrm{x}}(t)$ [W] is the internal heat generated by the object, if any, Y is the set of all elements y in thermal contact with x and R_{xy} [K/W] is the thermal resistance between x and y. Based on the setup described in Section II, the set of differential equations used to simulate the temperature dynamics of the three elements is:

$$\begin{cases} C_{\mathrm{c}}\dfrac{\mathrm{d}T_{\mathrm{c}}(t)}{\mathrm{d}t} = q_{\mathrm{gen}}(t) + \dfrac{T_{\mathrm{a}}(t)-T_{\mathrm{c}}(t)}{R_{\mathrm{ca}}} \\ C_{\mathrm{a}}\dfrac{\mathrm{d}T_{\mathrm{a}}(t)}{\mathrm{d}t} = \dfrac{T_{\mathrm{c}}(t)-T_{\mathrm{a}}(t)}{R_{\mathrm{ca}}} + \dfrac{T_{\mathrm{p}}(t)-T_{\mathrm{a}}(t)}{R_{\mathrm{ap}}} \\ C_{\mathrm{p}}\dfrac{\mathrm{d}T_{\mathrm{p}}(t)}{\mathrm{d}t} = \dfrac{T_{\mathrm{a}}(t)-T_{\mathrm{p}}(t)}{R_{\mathrm{ap}}} + \dfrac{T_{\mathrm{e}}(t)-T_{\mathrm{p}}(t)}{R_{\mathrm{pe}}} \end{cases} \tag{2}$$

where the subscripts c, a, p, and e indicate cell, aluminum, plexiglass and environment, respectively, $q_{\mathrm{gen}}(t)$ is the internal heat generated by the Li-ion cell, R_{ca} is the cell-aluminum thermal resistance, R_{ap} is the aluminum-plexiglass resistance and R_{pe} is the convective resistance between the plexiglass and the surrounding air.

The thermal model can be visualized through the equivalent electrical circuit in Fig. 3. where the currents represent heat fluxes, voltages represent temperatures, capacitors represent heat capacities and resistances represent thermal resistances. Accordingly, the cell heat is pictured as a current generator and the ambient temperature, which is assumed to be a constant value, is depicted as a voltage generator.

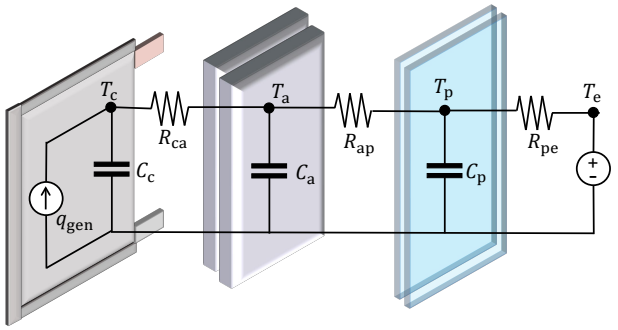

Fig. 3. Circuital representation of the thermal model.

The heat generated in lithium-ion cells is typically computed as the sum of two contributions [24]: the first, and major, is the product of current $I(t)$ and overpotential $\eta(t) = (V(t)-V_{\mathrm{ocv}}(t))$, where $V_{\mathrm{ocv}}(t)$ is the cell Open-Circuit Voltage (OCV). The second is commonly referred to as entropic heat generation and is computed as $I(t)T_{\mathrm{c}}(t)\mathrm{d}V_{\mathrm{ocv}}(t)/\mathrm{d}T_{\mathrm{c}}(t)$. The experimental investigation of the entropic heat coefficient $\mathrm{d}V_{\mathrm{ocv}}(t)/\mathrm{d}T_{\mathrm{c}}(t)$ has been exhaustively carried out in recent literature [25]–[28]. In [25], for example, temperature dynamics with and without entropic contribution are compared over a cycle of charge and discharge, interspersed with long relaxations: although the full model predicts local temperature fluctuations with high precision, the overpotential-only formulation already succeeds in fitting the measurements with satisfactory accuracy. In [26], entropic and overpotential heat are compared during C-Rate tests: when SoC is above 20%, the entropic contribution is shown to be negligible. This result is confirmed in most of the reviewed literature works: the entropic coefficient becomes meaningful in the total heat computation only at low SoC. Given that, in this work, the heat generated is computed as:

$$q_{\mathrm{gen}}(t) = I(t)\eta(t) = I(t)(V(t)-V_{\mathrm{ocv}}(t)). \tag{3}$$

The OCV is then expressed as a function of the cell's State of Charge (SoC). Given the high linearity of the Open Circuit Voltage (OCV) for the pouch cell under test, a third-order polynomial was deemed sufficient to accurately describe the relationship between $V_{\mathrm{ocv}}(t)$ and $\mathrm{SoC}(t)$:

$$V_{\mathrm{ocv}}(t) = \sum_{i=0}^{3} a_i \mathrm{SoC}(t)^i. \tag{4}$$

Finally, $\mathrm{SoC}(t)$ is computed with *Coulomb Counting* open-loop current integration:

$$\mathrm{SoC}(t) = \mathrm{SoC}_0 - \int_0^t \frac{I(t)}{3600\,Q_{\mathrm{nom}}}\mathrm{d}t, \tag{5}$$

where SoC_0 is the SoC at the beginning of each experiment and Q_{nom} is the nominal capacity of the cell, obtained with a capacity test. *Coulomb Counting* is generally used as a groundtruth for estimating the SoC under controlled laboratory conditions, when SoC_0 is known and the current is reliably measured by a BTE, as in this case. All differential equations mentioned so far are approximated through finite differences and implemented in MATLAB.

IV. Model Identification

Model parameters can be divided into two categories: electrical parameters, *i.e.*, the coefficients a_i of the $V_{\mathrm{ocv}}(\mathrm{SoC})$ curve, and thermal parameters, which characterize the temperature dynamics of the three objects, *i.e.*, the thermal capacities C_{x} and the contact resistances R_{xj}. The model identification is achieved in two sequential steps. In the first step, the OCV curve is identified. Characterization of OCV is a simple task, often addressed in the literature whenever an Equivalent Circuit Model (ECM) is identified [29]–[31]. In this work, a full constant discharge at low C-Rate is

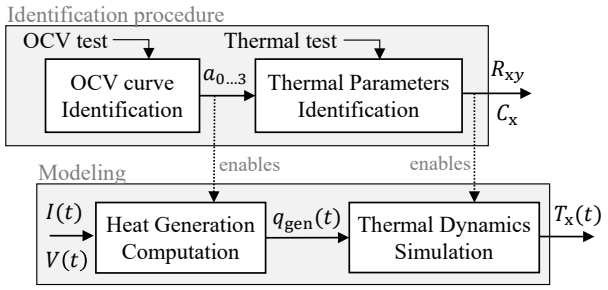

Fig. 4. The two identification steps (top) with relative tests and parameters identified and the two sub-models (bottom) enabled.

employed for this purpose. Knowing the OCV parameters of the cell, then, the overpotential heat can be computed using voltage measurement $V(t)$, current measurement $I(t)$ and $V_{\mathrm{ocv}}(t)$ computed through (5) and (4). In the second step, the characterization of thermal parameters is carried out with a test designed specifically to excite the temperature dynamics of the elements under analysis. Finally, the set of differential equations (2) can be simulated. The identification procedure, with the relative tests, and the model parts enabled by the two steps, are schematized in Fig.4.

A. OCV Curve Identification

The OCV curve is characterized by a C/10 discharge. Indeeed, a galvanostatic discharge at very low current intensity allows a good estimation of the the open-circuit voltage [32], especially for low-resistance cells. After a complete charge, the cell is completely discharged for about 10 hours at room temperature. The coefficients of the OCV curve are optimized by solving the following least squares problem, which minimizes, in the SoC domain, the distance between the polynomial formulation (4) and the measured voltage:

$$\begin{aligned} &\underset{a_1,a_2,a_3,a_4}{\text{minimize}} \quad \sum_{t=0}^{T}\left[\left(V_{\mathrm{C10}}(\mathrm{SoC(t)}) - V_{\mathrm{ocv}}(\mathrm{SoC(t)})\right)^2\right] \\ &\text{subject to} \quad (4),\ (5) \end{aligned} \tag{6}$$

where T is the duration of the discharge and V_{C10} is the measured voltage. For the reasons mentioned in Section II, the optimal parameters are not discussed.

B. Thermal Parameters Identification

The thermal identification test is designed by interspersing a current profile from a high-performance automotive application, consisting of both discharge and regenerative events, with relaxation periods. The latter are decisive for the identification of the system parameters: in these time frames the input variable does not influence the system's dynamics ($I(t) = 0 \Rightarrow q_{\mathrm{gen}}(t) = 0$) and the temperature trajectories $T_{\mathrm{x}}(t)$ depend solely on the parameters $C_{\mathrm{x}}, R_{\mathrm{xy}}$ and the state of the system at the beginning of the relaxations. The initial state of the system is controlled: the test is launched only when (*i*) the cell and the fixture elements are at the same equilibrium temperature, *i.e.*, the set-point of the thermal chamber, and (*ii*) the cell is at the pre-defined state of charge.

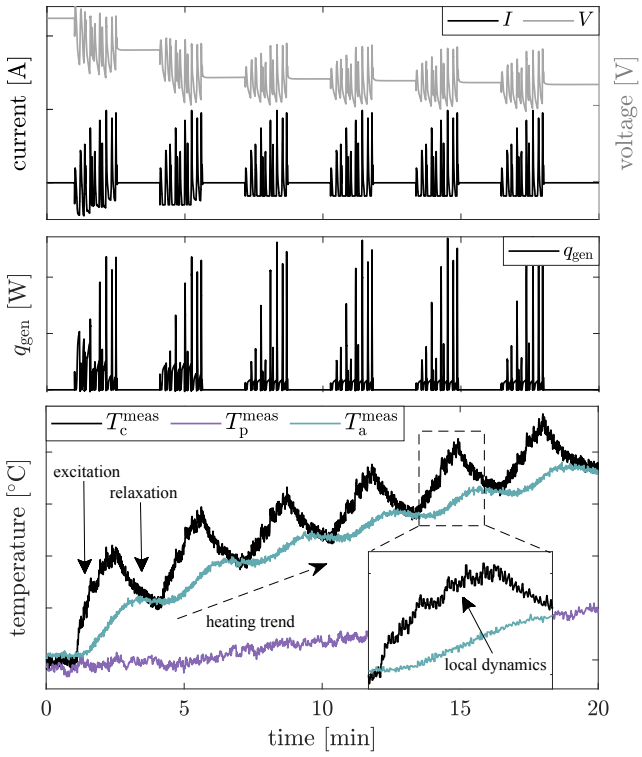

Fig. 5. Thermal identification test. From top to bottom: current (black) and voltage (grey) profiles, heat computed with (3), temperatures of the three objects (in the zoom: detail of the cell's local temperature fluctuations). The scale of the y-axis is hidden due to confidentiality constraints.

Current, voltage and simulated heat profile are shown, together with the temperature evolutions, in Fig. 5. The following features can be appreciated:

- cell's temperature alternates between excitations and relaxations, in accordance with the heat generated;
- during excitations, local temperature spikes, caused by current pulses, are visible;
- the aluminum acts as a filter with respect to the cell. The same is true with plexiglass, but it experiences a milder temperature increment;
- the duration of relaxations is designed short enough to cause overall warming of the setup.

Defining θ as the vector of unknown parameters:

$$\theta = [C_{\mathrm{c}},\, C_{\mathrm{a}},\, C_{\mathrm{p}},\, R_{\mathrm{ca}},\, R_{\mathrm{ap}},\, R_{\mathrm{pe}}]\,. \tag{7}$$

The set of optimal thermal parameters P^* is found solving the following nonlinear least squares problem (8), which minimizes the error between the measured and model-simulated temperature of the three objects:

$$\begin{aligned} &\underset{\theta}{\text{minimize}} \quad \sum_{x=\{\mathrm{c,a,p}\}}\sum_{t=0}^{T}\left[\left(T_{\mathrm{x}}^{\mathrm{meas}}(t) - T_{\mathrm{x}}(t)\right)^2\right] \\ &\text{subject to} \quad (2),\ (3),\ (4),\ (5) \end{aligned} \tag{8}$$

where $T_{\mathrm{x}}^{\mathrm{meas}}$ is the measured temperature profile for the object x and T_{x} is the simulated temperature profile. The nonlinear problem is solved via MATLAB *fmincon*.

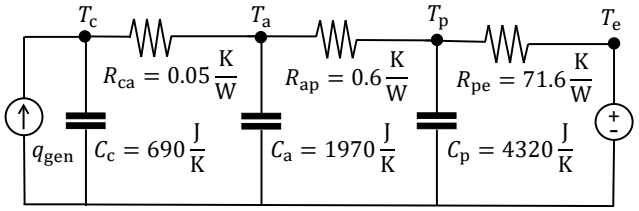

Fig. 6. Values of the optimal thermal parameters within the equivalent circuital representation in Fig.3.

The values of θ^* are displayed in Fig.6. The thermal capacity of the cell is found to be 690 J/K. This is the only parameter, among those identified, that is independent of the fixture device and pertains solely to the cell, and can therefore be reused in different simulation frameworks. Aluminum and plexiglass plates show higher thermal capacities (1970 J/K and 4320 J/K respectively): considering their dimensions, these values are consistent with the specific capacities of the two materials. The resistances reveal significant thermal contact between aluminum and cell (0.05 W/K), also due to sandwich compression. Finally, considerable thermal resistance is found between aluminum and plexiglass plates (0.6 W/K), a symptom of thermal insulation due to the poor conductivity of plexiglass.

The model shows an accurate prediction of the temperatures over time: simulation and measures are compared in Fig. 7. The satisfactory performance is confirmed by the evaluation of RMSE between measurements and simulations (cell: 0.11°C, aluminum: 0.06°C, plexiglass: 0.08°C).

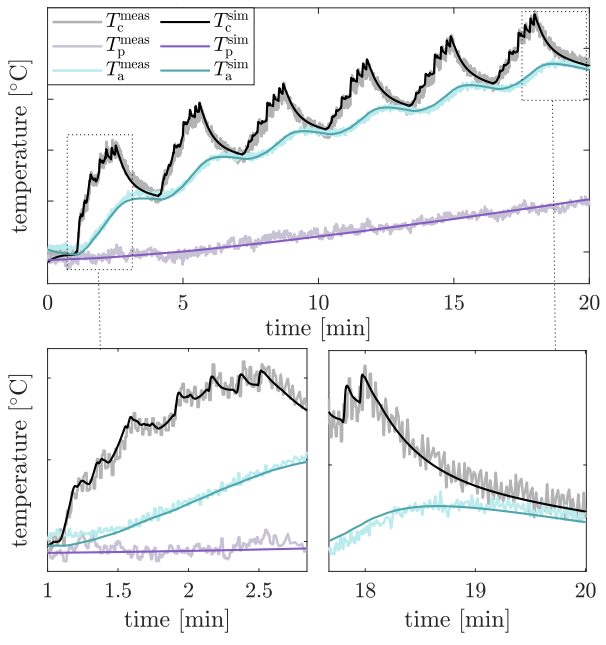

Fig. 7. Thermal identification test. Top: measured temperatures (faded lines) and corresponding simulated temperatures (sharp lines). Bottom: zooms of the first excitement (left) and the fitting of the last relaxation (right). The scale of the y-axis is hidden due to confidentiality constraints.

V. Model Validation

The model is finally validated with a different current profile. The input current and measured voltage, the computed heat and the temperature trajectories (measured and simulated) are displayed in Fig. 8. In contrast to the identification profile, the cell is subjected to a continuous excitation current with discharge and charge events, still taken from an automotive application, programmed to avoid a crossing of the maximum and minimum cell voltage limits and to ensure that the state of charge is maintained within certain limits. The following features can be noticed:

- both cell and aluminum temperatures exhibit a constant heating trend, consistent with the imposed constant excitation. ;
- small temperature ripples, given by current peaks, are visible on the cell temperature;
- as in the identification test, aluminum blocks and plexiglass plates act as temperature filters.

For this validation profile, the model prediction shows a slight drift from the measurement: after about 18 minutes of heating, the model error reaches the value of 0.5°C (cell). In general, the performance of the model is confirmed to be satisfactory with RMSE less than 0.4°C. Specifically, for the three objects, the RMSE is: 0.31°C (cell), 0.22°C (aluminum) and 0.21°C (plexiglass).

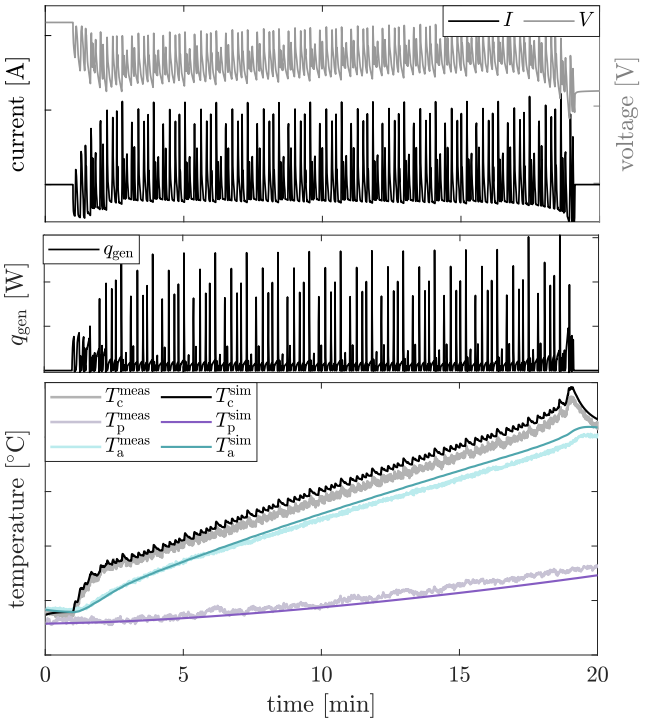

Fig. 8. Thermal model validation test. From top to bottom: measured current (black) and voltage (grey) profiles; heat computed with (3); measured (faded lines) and predicted (sharp lines) temperatures of the three objects. The scale of the y-axis is hidden due to confidentiality constraints.

VI. Conclusions

This paper presents a comprehensive analysis and experimental validation of a multi-element lumped-parameter thermal model for pouch-type lithium-ion battery cells and their containment assembly. The model is aimed at capturing the heat transfer dynamics among various components in the testing fixture, allowing for (*i*) the understanding of the thermal impact of each element and (*ii*) the identification of some cell-related parameters of interest, such as its thermal capacity. The identified model showed its accuracy and reliability in predicting temperature dynamics pouch cells under compression fixture conditions. The proposed approach, combining overpotential-driven heat generation with a lumped-parameter thermal model, holds promise for enhancing the efficiency and precision of thermal management in pouch-type cells. These results contribute to the broader goal of improving battery safety and performance, which is crucial for the growing electric vehicle industry and renewable energy applications.

References

[1] L. Sun, Y. Liu, R. Shao, J. Wu, R. Jiang, and Z. Jin, "Recent progress and future perspective on practical silicon anode-based lithium ion batteries," *Energy Storage Materials*, vol. 46, pp. 482–502, 2022.

[2] F. Zhao, J. Xue, W. Shao, H. Yu, W. Huang, and J. Xiao, "Toward high-sulfur-content, high-performance lithium-sulfur batteries: Review of materials and technologies," *Journal of Energy Chemistry*, vol. 80, pp. 625–657, 2023.

[3] S. Kalnaus, L. E. Asp, J. Li, G. M. Veith, J. Nanda, C. Daniel, X. C. Chen, A. Westover, and N. J. Dudney, "Multifunctional approaches for safe structural batteries," *Journal of Energy Storage*, vol. 40, p. 102747, 2021.

[4] X. Lin, Y. Kim, S. Mohan, J. B. Siegel, and A. G. Stefanopoulou, "Modeling and estimation for advanced battery management," *Annual Review of Control, Robotics, and Autonomous Systems*, vol. 2, no. 1, pp. 393–426, 2019.

[5] Q. Wang, P. Ping, X. Zhao, G. Chu, J. Sun, and C. Chen, "Thermal runaway caused fire and explosion of lithium ion battery," *Journal of Power Sources*, vol. 208, pp. 210–224, 2012.

[6] A. A. Hussein, "Experimental modeling and analysis of lithium-ion battery temperature dependence," pp. 1084–1088, 2015.

[7] T. Waldmann, M. Wilka, M. Kasper, M. Fleischhammer, and M. Wohlfahrt-Mehrens, "Temperature dependent ageing mechanisms in lithium-ion batteries – a post-mortem study," *Journal of Power Sources*, vol. 262, pp. 129–135, 2014.

[8] M. Wang and H.-X. Li, "Real-time estimation of temperature distribution for cylindrical lithium-ion batteries under boundary cooling," *IEEE Transactions on Industrial Electronics*, vol. 64, no. 3, pp. 2316–2324, 2017.

[9] M. Corno, "Efficient control-oriented coupled electrochemical thermal modeling of li-ion cells," *IEEE Transactions on Industrial Electronics*, vol. 68, no. 8, pp. 7024–7033, 2021.

[10] A. Trivella, M. Corno, S. Radrizzani, and S. M. Savaresi, "Non-invasive experimental identification of a single particle model for lifepo4 cells," *IFAC-PapersOnLine*, 2023, the 22nd World Congress of the International Federation of Automatic Control (in press, preprint available on arXiv 2306.14195).

[11] E. Miguel, G. L. Plett, M. S. Trimboli, L. Oca, U. Iraola, and E. Bekaert, "Review of computational parameter estimation methods for electrochemical models," *Journal of Energy Storage*, vol. 44, p. 103388, 2021.

[12] M. A. Perez Estevez, S. Calligaro, O. Bottesi, C. Caligiuri, and M. Renzi, "An electro-thermal model and its electrical parameters estimation procedure in a lithium-ion battery cell," *Energy*, vol. 234, p. 121296, 2021.

[13] Y. Kim, S. Mohan, J. Siegel, A. Stefanopoulou, and Y. Ding, "The estimation of temperature distribution in cylindrical battery cells under unknown cooling conditions," *IEEE Transactions on Control Systems Technology*, vol. 22, pp. 1–1, 11 2014.

[14] N. Abdul Samad, B. Wang, J. Siegel, and A. Stefanopoulou, "Parameterization of battery electro-thermal models coupled with finite element flow models for cooling," *Journal of Dynamic Systems, Measurement, and Control*, vol. 139, 01 2017.

[15] B. Choi, M. Lee, S.-G. Woo, G. Jeong, H. Lee, J.-N. Lee, and J.-S. Yu, "Importance of uniformly redistributing external pressure on cycling of pouch-type li-metal batteries," *Korean Journal of Chemical Engineering*, vol. 40, 02 2023.

[16] X. Du, Y. Hu, S.-Y. Choe, T. R. Garrick, and M. A. Fernandez, "Characterization and analysis of the effect of pressure on the performance of a large format nmc/c lithium-ion battery," *Journal of Power Sources*, vol. 573, p. 233117, 2023.

[17] A. S. Mussa, M. Klett, G. Lindbergh, and R. W. Lindström, "Effects of external pressure on the performance and ageing of single-layer lithium-ion pouch cells," *Journal of Power Sources*, vol. 385, pp. 18–26, 2018.

[18] L. Aiello, P. Ruchti, S. Vitzthum, and F. Coren, "Influence of pressure, temperature and discharge rate on the electrical performances of a commercial pouch li-ion battery," *Batteries*, vol. 10, no. 3, p. 72, 2024.

[19] G. Vertiz, M. Oyarbide, H. Macicior, O. Miguel, I. Cantero, P. Fernandez de Arroiabe, and I. Ulacia, "Thermal characterization of large size lithium-ion pouch cell based on 1d electro-thermal model," *Journal of Power Sources*, vol. 272, pp. 476–484, 2014.

[20] A. Samba, N. Omar, H. Gualous, Y. Firouz, P. Van den Bossche, J. Van Mierlo, and T. I. Boubekeur, "Development of an advanced two-dimensional thermal model for large size lithium-ion pouch cells," *Electrochimica Acta*, vol. 117, pp. 246–254, 2014.

[21] K. Murashko, J. Pyrhönen, and L. Laurila, "Three-dimensional thermal model of a lithium ion battery for hybrid mobile working machines: Determination of the model parameters in a pouch cell," *IEEE Transactions on Energy Conversion*, vol. 28, no. 2, pp. 335–343, 2013.

[22] S. Goutam, A. Nikolian, J. Jaguemont, J. Smekens, N. Omar, P. Van Dan Bossche, and J. Van Mierlo, "Three-dimensional electro-thermal model of li-ion pouch cell: Analysis and comparison of cell design factors and model assumptions," *Applied Thermal Engineering*, vol. 126, pp. 796–808, 2017.

[23] M. Mastali, E. Foreman, A. Modjtahedi, E. Samadani, A. Amirfazli, S. Farhad, R. A. Fraser, and M. Fowler, "Electrochemical-thermal modeling and experimental validation of commercial graphite/lifepo4 pouch lithium-ion batteries," *International Journal of Thermal Sciences*, vol. 129, pp. 218–230, 2018.

[24] K. Thomas, C. Bogatu, and J. Newman, "Measurement of the entropy of reaction as a function of state of charge in doped and undoped lithium manganese oxide," *Journal of The Electrochemical Society*, vol. 148, pp. A570–A575, 06 2001.

[25] M. Shadman Rad, D. Danilov, M. Baghalha, M. Kazemeini, and P. Notten, "Adaptive thermal modeling of li-ion batteries," *Electrochimica Acta*, vol. 102, pp. 183–195, 2013.

[26] Y. Abdul-Quadir, T. Laurila, J. Karppinen, K. Jalkanen, K. Vuorilehto, L. Skogström, and M. Paulasto-Kröckel, "Heat generation in high power prismatic li-ion battery cell with limnnicoo2 cathode material," *International Journal of Energy Research*, vol. 38, no. 11, pp. 1424–1437, 2014.

[27] N. Damay, C. Forgez, M.-P. Bichat, and G. Friedrich, "A method for the fast estimation of a battery entropy-variation high-resolution curve – application on a commercial lifepo4/graphite cell," *Journal of Power Sources*, vol. 332, pp. 149–153, 2016.

[28] K. Murashko, A. Mityakov, V. Mityakov, S. Sapozhnikov, J. Jokiniemi, and J. Pyrhönen, "Determination of the entropy change profile of a cylindrical lithium-ion battery by heat flux measurements," *Journal of Power Sources*, vol. 330, pp. 61–69, 2016.

[29] B. Yann Liaw, G. Nagasubramanian, R. G. Jungst, and D. H. Doughty, "Modeling of lithium ion cells—a simple equivalent-circuit model approach," *Solid State Ionics*, vol. 175, no. 1, pp. 835–839, 2004.

[30] S. Nejad, D. Gladwin, and D. Stone, "A systematic review of lumped-parameter equivalent circuit models for real-time estimation of lithium-ion battery states," *Journal of Power Sources*, vol. 316, 2016.

[31] S. S. Madani, E. Schaltz, and S. Knudsen Kær, "An electrical equivalent circuit model of a lithium titanate oxide battery," *Batteries*, vol. 5, no. 1, 2019.

[32] Z. Ren, C. Du, Z. Wu, J. Shao, and W. Deng, "A comparative study of the influence of different open circuit voltage tests on model-based state of charge estimation for lithium-ion batteries," *International Journal of Energy Research*, vol. 45, no. 9, pp. 13 692–13 711, 2021.